The impact of anion ordering on octahedra distortion and phase transitions in $SrTaO_2N$ and $BaTaO_2N$

Authors

Chun-Hai Wang[a], Brendan J. Kennedy[a]*, André L. Menezes de Oliveira[a], Julia Polt[a] and Kevin Steven Knight[bc]

[a]School of Chemistry, The University of Sydney, Sydney, NSW, 2006, Australia

[b]Department of Earth Sciences, The Natural History Museum, Cromwell Road, London, SW7 5BD, United Kingdom

[c]Department of Earth Sciences, University College London, Gower Street, London, WC1E 6BT, United Kingdom

Correspondence email: brendan.kennedy@sydney.edu.au

Synopsis Anion (O/N) ordering was observed in $BaTaO_2N$ and $SrTaO_2N$. A further Ta-O/N octahedra displacement (rotation about the *c* axis) distortion was observed in $SrTaO_2N$.

Abstract In this work, we synthesized $BaTaO_2N$ and $SrTaO_2N$ using a two-step high temperature solid state reaction method and analysed the structural distortions, relative to the ideal cubic perovskite structure, according to group theory. From a complete distortion analysis/refinement using high resolution neutron diffraction data in the temperature range 8 K to 613 K, we identified tetragonal structures for $BaTaO_2N$ [*P*4/*mmm* (No 123)] and $SrTaO_2N$ [*I*4/*mcm* (No 140)]. In contrast to an anion-disordered cubic perovskite ($Pm\bar{3}m$ No 221) with Ta at the cell center, both systems show a site preference for oxygen anions in the two opposite corners (along the *c* axis) of the Ta-O/N octahedra rather than the four square corners in the *ab* plane ($\mathbf{\Gamma}_3^+$ occupancy distortion), which induces a tetragonal elongation of the unit cell with the *c* axis being longer than the *a* axis. A further Ta-O/N octahedra displacement [$\mathbf{R}_5^-$(a,0,0), rotation about the *c* axis] distortion was observed in $SrTaO_2N$. This distortion mode is accompanied by an increased unit cell distortion that decreases as the temperature increases. Ultimately a second-order phase transition caused by the loss of the $\mathbf{R}_5^-$(a,0,0) mode was observed at 400 – 450 K.

Keywords: anion ordering, distortion, oxynitride

1. Introduction

Mixed anion materials, in particular oxynitrides, are attracting considerable attention for their novel properties. $SrTaO_2N$ and $BaTaO_2N$ are two typical perovskite oxynitrides that have been widely studied due to their promising properties that include, semiconductivity(Kim *et al.*, 2004), dielectric relaxation(Kim *et al.*, 2004, Sun *et al.*, 2014, Hinuma *et al.*, 2012, Masubuchi, 2013) and photocatalytic activity(Higashi *et al.*, 2008, Higashi *et al.*, 2013, Higashi *et al.*, 2015, Oehler & Ebbinghaus, 2016, Ueda *et al.*, 2015). Evidently the distortion of the octahedra in perovskite oxynitrides is a key parameter in understanding their interesting properties. Thus, a careful and systematic study of the Ta-O/N octahedra distortion in $SrTaO_2N$ and $BaTaO_2N$ is likely to enhance our understanding of these fascinating materials.

$SrTaO_2N$ and $BaTaO_2N$ are also good structural models to study O/N anion ordering in perovskites and probe the structural distortions that arise from such ordering. $BaTaO_2N$ has been reported to adopt an ideal cubic perovskite structure ($Pm\bar{3}m$ No 221) with the O/N anions completely disordered in the anion octahedra (Kim *et al.*, 2004, Pors *et al.*, 1988) (Figure 1). The situation of $SrTaO_2N$ is more complex, and several structural models have been reported: *I*4/*mcm* (No 140) (Günther *et al.*, 2000, Zhang *et al.*, 2011, Kim *et al.*, 2004, Clarke *et al.*, 2002), *I*112/*m* (No 12)(Yang *et al.*, 2011) and *Fmmm* (No 69)(Clark *et al.*, 2013). Wolff and Dronskowski investigated the structure of $SrTaO_2N$ and $BaTaO_2N$ using first-principle and molecular dynamics calculations based on density functional theory (DFT) and suggested that for both oxynitrides the space group should be orthorhombic in $Pmc2_1$ (No 26)(Wolff & Dronskowski, 2008). The major difference among the various structural models described for $SrTaO_2N$ is the nature of the O/N ordering and the distortion (bond angles/distance anisotropy) of the Ta-O/N octahedra. For example, Günther *et al*. reported a completely ordered structural model with site s1 (Figure 1) occupied by N and the other anion sites occupied by O(Günther *et al.*, 2000). Meanwhile, Clark *et al*. described another ordering pattern with site s1 (Figure 1) mainly occupied by O (~95%) and the other anion sites randomly occupied by O/N(Clark *et al.*, 2013). Other works have suggested only partial O/N ordering (~75% O at site s1) (Clarke *et al.*, 2002, Yang *et al.*, 2011, Zhang *et al.*, 2011) in the Ta-O/N octahedra. All the models reported to date gave similar distortion of the Ta-O/N octahedra.

The local structure of the Ta-O/N octahedra in $SrTaO_2N$ and $BaTaO_2N$ was also studied by DFT calculations(Fang *et al.*, 2003, Page *et al.*, 2007, Wolff & Dronskowski, 2008, Ravel *et al.*, 2006), extended X-ray absorption fine structure (EXAFS)(Ravel *et al.*, 2006), and neutron pair distribution function (PDF) analysis(Page *et al.*, 2007). These confirmed the *cis*-TaO_4N_2 configuration in both $SrTaO_2N$ and $BaTaO_2N$. Thus, the possible N/O ordering patterns (Attfield, 2013, Yang *et al.*, 2011, Zhang *et al.*, 2011) in a long range average structure are built upon a *cis*-TaO_4N_2 configuration and there should be more oxygen at the s1 site relative to the other sites illustrated in Figure 1.

The structures of $SrTaO_2N$ or $BaTaO_2N$ can be described as distortions from the ideal cubic perovskite structure (Figure 1), in which the O/N occupancy and atomic displacements are the distortion parameters (degrees of freedom). All possible distorted structures (complete base) can be derived using group theory analysis, from the parent structure, as long as the wave vector(s) is known(Campbell *et al.*, 2006). The distorted structure is caused by the action of one or more distortion modes, which have physical meanings in terms of the atomic interactions. Describing complex structures in terms of distortion modes has a significant advantage in that, under some circumstances, it can reduce the number of structural parameters and this can increase the reliability of the refined structural model (an application of Occam's razor to crystallographic analysis). It has previously been demonstrated that the structure analysis based on the symmetry-mode refinements is an effective and powerful method and has been successful used in the analysis of complex oxides including WO_3 and $Bi_2Sn_2O_7$ (Kerman *et al.*, 2012, Lewis *et al.*, 2016), although this approach does not appear to have been used in systems with mixed anions. Thus, a structure analysis of $SrTaO_2N$ and $BaTaO_2N$ based on the distortion refinement is helpful for more reliable structure determination of them. Using =group theory, Talanov *et al*. have analysed all the 261 possible low symmetry structures caused by anion ordering in perovskite up to $2 \times 2 \times 2$ super cell (four vectors considered: **X**, **M**, **R**, and **Γ**) and summarized the reported experiment results (Talanov *et al.*, 2016). They supposed that the $SrMO_2N$ (M = Ta, Nb) compounds adopt $A^{1a}B^{1d}X^{1c}X^{2e}{}_2$ anion ordering. However, they did not analyse the complete distortions (ordering and displacement) for oxynitride perovskite by structure refinements, which would give more details on the nature and magnitude of the distortion modes.

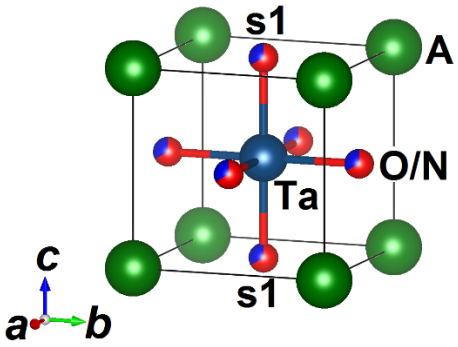

Figure 1. Representation of the perovskite structure of $ATaO_2N$. The mixed occupancy of O (red) and N (blue) is represented by the shading.

In the present work the temperature-dependent structural distortions of $SrTaO_2N$ and $BaTaO_2N$ have been studied using high resolution neutron diffraction data measured at fine temperature intervals between 8 K and ~600 K. The structures and phase transitions are described based on the distortion mode refinements.

2. Experimental section

Polycrystalline samples of $BaTaO_2N$ and $SrTaO_2N$ were synthesized in two steps. Initially a 1:2 (mole ratio) of Ta_2O_5 (Aithaca, 99.99%) and $SrCO_3$ (Aldrich, >99.9%) or $BaCO_3$ (Aithaca, 99.999%), all dried at 400 °C for 10 h before use, was weighed and ground. The well mixed powder was then calcined at 1100 °C for 36 h with an intermediate regrinding. After the calcination, the powder was confirmed as a single phase of $Sr_2Ta_2O_7$ or $Ba_2Ta_2O_7$ from powder X-ray diffraction (XRD) analysis. The precursor $Sr_2Ta_2O_7$ or $Ba_2Ta_2O_7$ was then put into an alumina boat and nitrided in a tube (squartz) furnace under a 300 ml/min NH_3 flow. The nitridation was conducted at 1000 °C for 24 h with an intermediate regrinding. After the nitridation, the white precursor changed to a bright orange ($SrTaO_2N$) or red brown ($BaTaO_2N$) product. The phases of samples prepared were determined from Rietveld refinement using synchrotron X-ray diffraction to be a major (~99% wt.) $SrTaO_2N$ or $BaTaO_2N$ phase and a minor (~1% wt.) Ta_3N_5 impurity phase.

Time-of-flight (TOF) powder neutron diffraction (ND) data of $BaTaO_2N$ (~7 g) and $SrTaO_2N$ (~7 g) samples were collected on the high resolution powder diffraction (HRPD) diffractometer at the ISIS facility of the Rutherford Appleton Laboratory (UK). The data collected using the backscattering (b1) and 90° (b2) detectors were analysed. The temperature range of interest, from 8 to 613 K, necessitated the use of both cryostat and furnace. The powdered samples were lightly packed into either an aluminium can of slab geometry for measurements in the cryostat (4.2 – 300 K), or a thin-walled 11 mm diameter vanadium can for analysis in the furnace (first at room temperature, followed by measurements from 373 to 613 K). The data were acquired for 2 - 4 h at RT (13°C, 286 K), 418 and 8K and 30 min/scan for the other temperatures.

The structure of $BaTaO_2N$ and $SrTaO_2N$ was investigated by Rietveld refinements against the b1 and b2 ND data) using TOPAS Academic (TA)(Coelho *et al.*, 2011, Evans, 2010). For the refinements the cubic disordered perovskite structure model was selected as parent structure (undistorted) and symmetry representation analysis was applied using ISODISTORT(Campbell *et al.*, 2006) according to the observed supercell reflections, to build and test the occupancy and displacement distortions against the RT and 300 K data. After the distortion was confirmed, a batch refinement using selected distortion models against the data at all temperatures was conducted to investigate the temperature dependent distortion transitions.

Room temperature oxygen and nitrogen K-edge X-ray absorption near edge spectra (XANES) of $BaTaO_2N$ and $SrTaO_2N$ were collected at the soft X-ray spectroscopy beamline of Australian Synchrotron. Finely ground powder was pressed onto a conducting carbon tape to form a homogenous layer. Due to the very small penetration depth of the selected soft X-rays, a careful thickness optimisation was necessary to ensure sure that there is no signal from the tape substrate. The tape was placed on the gold-coated disc. The spectra were collected with a vacuum lower than 10^{-9} mbar. The X-ray absorption spectra (530 – 600 eV for oxygen K-edge and 385 – 435 eV for nitrogen K-edge) were collected in a total fluorescence yield (TFY) mode with 0.1eV/step and the default collection

angle (55°) was selected. For each measurement, the spectra of reference (MnO for O K-edge and BN for N K-edge) was simultaneously measured to calibrate the energy.

Absorption/reflection spectra of $BaTaO_2N$ and $SrTaO_2N$ were measured using a CARY5000 UV-Vis-NIR spectrophotometer equipped with a Harrick Praying Mantis solid-state reflection accessory. The spectra were collected from 200 – 1500 nm with $BaSO_4$ as reference.

3. Results and discussion

Structure of $BaTaO_2N$. The structure of $BaTaO_2N$ has previously been reported to be an undistorted cubic perovskite (Pors *et al.*, 1988). No peaks indicative of supercell symmetry were observed in the current neutron diffraction data. The Rietveld refinement using the undistorted $Pm\bar{3}m$ model against the HRPD data gave R_{wp} factors of: 3.51% (overall), 4.46% (b1), 2.80% (b2) for the 8 K data and 3.64% (overall), 4.67% (b1), 2.83% (b2) for the 300 K data. A distortion analysis was undertaken and the resulting models tested by refinement against the HRPD data to test the possibility of small distortions of the perovskite structure from ordering of the N and O anions. Since no supercell reflections were observed in the diffraction data, the distortion vector should be $\mathbf{k}_{12}(0\ 0\ 0)$ ($\mathbf{\Gamma}$) and considering the distortion vector five distortion irreducible representations (IR) are possible(Campbell *et al.*, 2006): $\mathbf{\Gamma}_1^+$, $\mathbf{\Gamma}_3^+$, $\mathbf{\Gamma}_5^+$, $\mathbf{\Gamma}_4^-$, and $\mathbf{\Gamma}_5^-$. The model $\mathbf{\Gamma}_3^+$ (one internal parameter) gave a better refinement result against our ND data with R_{wp} factors: 3.46% (overall), 4.41% (b1), 2.76% (b2) for 8 K data and 3.58% (overall), 4.60% (b1), 2.77% (b2) for 300 K data. The overall R_{wp} factors of the other models are: 8K 3.50% ($\mathbf{\Gamma}_1^+$), 3.50% ($\mathbf{\Gamma}_5^+$), 3.48% ($\mathbf{\Gamma}_4^-$), 3.48% ($\mathbf{\Gamma}_5^-$) and 300K 3.62% ($\mathbf{\Gamma}_1^+$), 3.60% ($\mathbf{\Gamma}_5^+$), 3.58% ($\mathbf{\Gamma}_4^-$), 3.59% ($\mathbf{\Gamma}_5^-$). It should be noted that the $\mathbf{\Gamma}_4^-$, and $\mathbf{\Gamma}_5^-$ models give similar quality refinements to that of the $\mathbf{\Gamma}_3^+$ model but required more internal parameters (12 in $\mathbf{\Gamma}_4^-$ and 3 in $\mathbf{\Gamma}_5^-$).The refined profiles at 300 K are shown in Figure 2, and demonstrate this model provides an excellent fit to the data. The variable temperature (VT, 9 to 300 K) neutron diffraction data of $BaTaO_2N$ are shown in Figure S1 of the supporting information (SI). The distorted structural model can be described with an O/N ordering mode and the corresponding unit cell distortion from cubic to tetragonal in space group *P*4/*mmm* (No 123). Consideration of the most general order parameter direction of the two-dimensional IR $\mathbf{\Gamma}_3^+$, which has two O/N-ordering modes rather than just one and results in *Pmmm* symmetry, did not result in any improvement to the refinement. Nor did simultaneously invoking the other available gamma-point IR modes improve the refinement. Thus, it is concluded that the structure of $BaTaO_2N$ is tetragonal with one occupancy distortion mode from the O/N ordering. This is in agreement with the recent results of Talanov *et al.*, who described a "pure" $\mathbf{\Gamma}_3^+$ ordering distortion ($\boldsymbol{\tau}_5$ in Kovalev notation)(Talanov *et al.*, 2016). The refined $BaTaO_2N$ structure is shown in Figure 3 and the structural parameters are summarized in Table 1.

It is illustrative to consider the refined O/N occupancies. The negligible difference between the refined O/N occupancy at 300 K and 8 K is consistent with our expectation that the anions do not

have sufficient energy to hop between different sites at low temperatures, and that the anion distribution is frozen at a blocking temperature during the high temperature synthesis. Consequently, the O/N occupancy was fixed to the optimal fit obtained against the 300 K data for all the refinements against data measured at other temperatures. Compared with the random occupancy (O/N = 0.67/0.33) at both sites, the optimised tetragonal *P*4/*mmm* model in $BaTaO_2N$ shows that there is more oxygen [O/N = 0.87(2)/0.13(2)] at the two opposite corners of the Ta-O/N octahedra (along the *c* axis) and more nitrogen [O/N = 0.56(1)/0.44(1)] at the four square sites parallel to the *ab* plane. Thus, there are more *cis*-Ta-N bonds parallel to the *ab* plane than in either the *ac* or *bc* planes. A consequence of the O/N ordering is the slight difference observed between the *a* and *c* axis [~0.0037(1) Å at 9 K and ~0.0041(1) Å at 300 K]. However, it is impossible to determine which axis (*a* or *c*) is longer from current diffraction data. The overall R_{wp} factors of $a > c$ model at 8K and 300K are 3.47% and 3.59%, which are insufficient to distinguish this from the $a < c$ model described above. DFT calculations have shown the average *cis*-Ta-N bond distance is less than the average Ta-O bond distance (2.01 versus 2.12 Å) (Wolff & Dronskowski, 2008) reflecting the stronger Ta-N π bonds compared to the Ta-O π bonds. Since there are more Ta-N bonds in the *ab* plane, it is expected that the *a* axis should be shorter than the *c* axis for the tetragonal $BaTaO_2N$ unit cell and this assumption was used in developing the structural models.

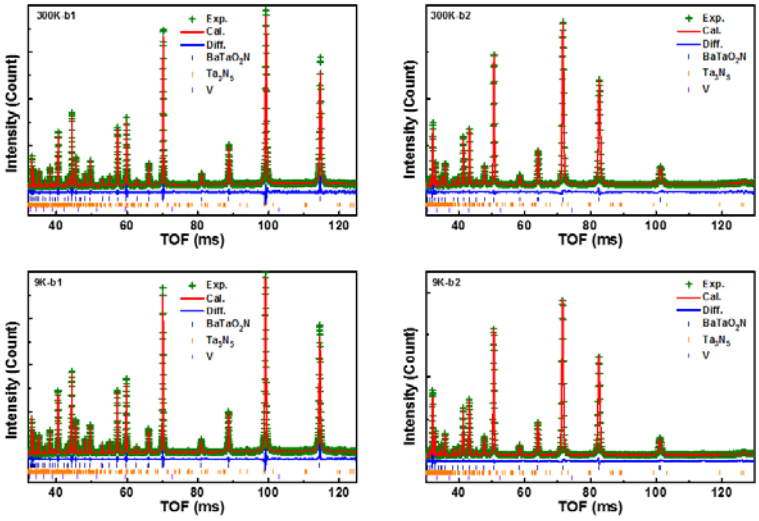

Figure 2. Observed, calculated and difference profiles of ND data for $BaTaO_2N$ at 9 K and 300 K using Γ_3^+ *P*4/*mmm* model. The short vertical marks are for the main tetragonal phase and for Ta_2N_5 and V (from the sample holder).

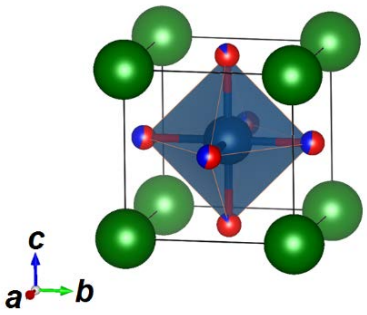

Figure 3. Representation of the crystal structure of $BaTaO_2N$. The large green spheres represent the Ba cations. The occupancy of O (red) and N (blue) is shown as a fraction of the small spheres in the TaO_4N_2 octahedron.

Table 1 Refined structural parameters for $BaTaO_2N$

T	9 K			300 K	
SG	*P*4/*mmm* (123)			*P*4/*mmm* (123)	
a (Å)	4.10502(6)			4.11061(6)	
c (Å)	4.10874(12)			4.11475(11)	
V (Å^3)	69.237(3)			69.527(3)	
	Coordinate	Occupancy	Beq(Å^2)	Occupancy	Beq(Å^2)
Ba	1a (0 0 0)	1	0.22(2)	1	0.48(2)
Ta	1d (½ ½ ½)	1	0.67(2)	1	0.84(2)
O/N(1)	2e (0 ½ ½)	0.58(1)/0.42(1)	0.58(2)	0.56(1)/0.44(1)	0.75(2)
O/N(2)	1c (½ ½ 0)	0.84(2)/0.16(2)	0.58(2)	0.87(2)/0.13(2)	0.75(2)

The temperature dependence of the refined unit cell parameters (*a*, *c*, *V*) are plotted in Figure 4. All the cell parameters increase with increasing temperature and the cell parameters can be described by a single term Einstein-type expression. The cell volume *V* against temperature (*T*) is well produced by an expression of the type:

$$\ln\left(\frac{V}{V_0}\right) = \frac{C\theta}{\exp\left(\frac{\theta}{T}\right)-1} \quad (1)$$

where *T* is temperature, *V* and V_0 are the cell volume at *T* and 0 K, *C* is a constant, and θ is the empirical saturation temperature. The fitted parameters are V_0 = 69.243(1) Å^3, $C = 2.05(1) \times 10^{-5}$ K^{-1} and θ = 243(5) K. The difference between *a* and *c* ($c - a = c_p - a_p$, where the subscript p refers to the

equivalent perovskite cell) can be considered as the degree of tetragonal distortion. This remains essentially constant as the temperature is increased from 9 to 300 K demonstrating the tetragonal unit cell distortion is a consequence of O/N ordering, which does not change over the temperature range investigated.

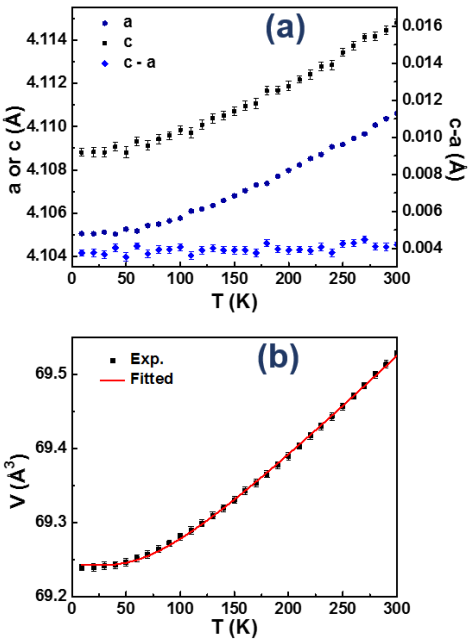

Figure 4. Temperature dependence of the tetragonal unit cell parameters and equivalent unit cell volume for $BaTaO_2N$ estimated from Rietveld refinements of PND data.

Structure of $SrTaO_2N$. Neutron diffraction patterns of $SrTaO_2N$ at 8K are shown in Figure 5. The ND peaks of $SrTaO_2N$ are noticeably broader than those of $BaTaO_2N$, indicating that more strain exists in $SrTaO_2N$, presumably due to the different ionic size of the Sr^{2+} and Ba^{2+} cations (tolerance factor 0.98 for $SrTaO_2N$ versus 1.03 for $BaTaO_2N$)(Wolff & Dronskowski, 2008). The red curves in Figure 5 are simulated from the undistorted cubic structure model. Five extra peaks labelled (pk1 - pk5) are evident in the figure. Comparing data measured at 300 K data (with cryostat) and 13 °C data (~286 K, without cryostat), see Figure S2, demonstrates peak pk2 is from the cryostat. This was further confirmed from the RT synchrotron XRD measurements, where this peak was not observed. The remaining peaks demonstrate the need to describe the structure in terms of a larger unit cell. The variable temperature neutron diffraction data of $SrTaO_2N$ is shown in Figure S3. The normalized intensities of the four additional "superlattice" reflections, estimated by peak fitting, are also plotted in Figure 5. The intensity of all these peaks decreases as the temperature increases and all of them are no longer apparent in the data measured above ~450 K, indicating that the four peaks should come from the same distortion. These peaks can be indexed by the vector $\mathbf{k}_{13}$(½, ½, ½) (**R**) relative to the

ideal cubic undistorted parent structure. Considering the distortions vectors (base) the **R**-point has five irreducible representation (IR)(Campbell *et al.*, 2006): $\mathbf{R}_5^+$, $\mathbf{R}_2^-$, $\mathbf{R}_3^-$, $\mathbf{R}_4^-$, and $\mathbf{R}_5^-$. With the exception of $\mathbf{R}_2^-$, all of these IRs are compatible with the O/N ordering distortion IR $\mathbf{\Gamma}_3^+$ identified in $BaTaO_2N$ (i.e. as a secondary order parameter, $\mathbf{\Gamma}_3^+$ is consistent with symmetry of the primary **R**-point order parameter). The general Ta-O/N octahedra displacement distortions of these IRs are sketched in Figure 6. The orientations of these distortions (vector) relative to the octahedra can be different or combined. It should be noted that most of the previously reported structural models for $SrTaO_2N$ can be described as arising from a combination of a $\mathbf{R}_5^-$ displacement distortion and $\mathbf{\Gamma}_3^+$ O/N occupancy distortion. However, the structural model reported by Clark *et al.*(Clark *et al.*, 2013) is a combination of $\mathbf{R}_5^-$ and $\mathbf{R}_4^-$ and two $\mathbf{\Gamma}_3^+$ O/N occupancy distortions.

We tested the possible distortion models of $SrTaO_2N$ by Rietveld refinements against the 13 °C and 8 K ND data. For each model, the occupancy distortion and displacement distortion were considered. A combined distortion model (two vectors) of $\mathbf{R}_5^-$ and $\mathbf{R}_4^-$ was also tested. The overall R_{wp} factors of the best refinements of these distortions are shown in Figure 7 (a) and (b). The $\mathbf{R}_5^-$ distortion gave the best refinement result showing the lowest R_{wp} factor and there is no significant improvement when both $\mathbf{R}_5^-$ and $\mathbf{R}_4^-$ were considered. Thus, we believe it is appropriate to describe the distortion of $SrTaO_2N$ in terms of the $\mathbf{R}_5^-$, which is dominated by the out-of-phase rotation distortion of Ta-O/N octahedra, and O/N ordering. The various order parameter directions of the three-dimensional $\mathbf{R}_5^-$ IR lead to six different structural models, each having different structural degrees of freedom, supercell basis and space-group symmetry. The appropriate crystallographic space groups are *I*4/*mcm* (No 140) associated with order parameter direction (a,0,0) of $\mathbf{R}_5^-$, *Imma* (No 74), $R\bar{3}c$ (No 167), *C*2/*m* (No 12), *C*2/*c* (No 15), and $P\bar{1}$ (No 2). Rietveld refinements of 8 K ND data (showing largest distortion) based on these different symmetries were tested with the overall R_{wp} factors shown in Figure 7 (c). The structure model with symmetry *C*2/*m* (No 12) and $P\bar{1}$ (No 2) give a best fit to the experiment data with R_{wp} factors 4.45% and 4.48%. However, the much higher symmetry structure model *I*4/*mcm* (No 140) gave a similar overall R_{wp} factor 4.52%. Considering the refinement uncertainty, caused by strain induced peak broadening, the structure model *I*4/*mcm* (No 140) which involves fewer variable parameters (Occam's razor) was selected for the subsequent structural refinements. It should be noted that these distortions agree with the group theory analysis of Talanov *et al.*, which are described as tilting $\boldsymbol{\tau}_8$ and permutation (ordering) $\boldsymbol{\tau}_5$ modes(Talanov *et al.*, 2016) in the notation of Kovalev. ISODISTORT indicates that a transition involving $\mathbf{R}_5^-$(a,0,0) to $\mathbf{\Gamma}_3^+$(a,0,0) is allowed to be continuous by both Landau and renormalization group theory. Both *C*2/*m* and *I*4/*mcm* structure models are given as CIF files in the SI. The refinement profiles at selected temperature using model *I*4/*mcm* (No 140) are shown in Figure 8 and the refined structural parameters are given in Table 2 (cif files are given in SI). Considering the ordering of the O/N anions, the s1 site (4*a* of *I*4/*mcm*), Figure 1, is fully occupied by oxygen and the other sites (8*h* of *I*4/*mcm*) are randomly occupied by O/N (1:1). A small tetragonal

distortion of the unit cell is evident. This can be described by a distortion parameter $\delta = c/2 - a/\sqrt{2} = c_p - a_p$ and this is observed to increase as the temperature is decreased δ = 0.006(1), 0.083(1), 0.018(1) Å at 145 °C (418 K), 13 °C (286 K), 8K respectively. The δ parameter is expected to be positive, i.e. $c_p / a_p > 1$ for the same reasons described above for $BaTaO_2N$.

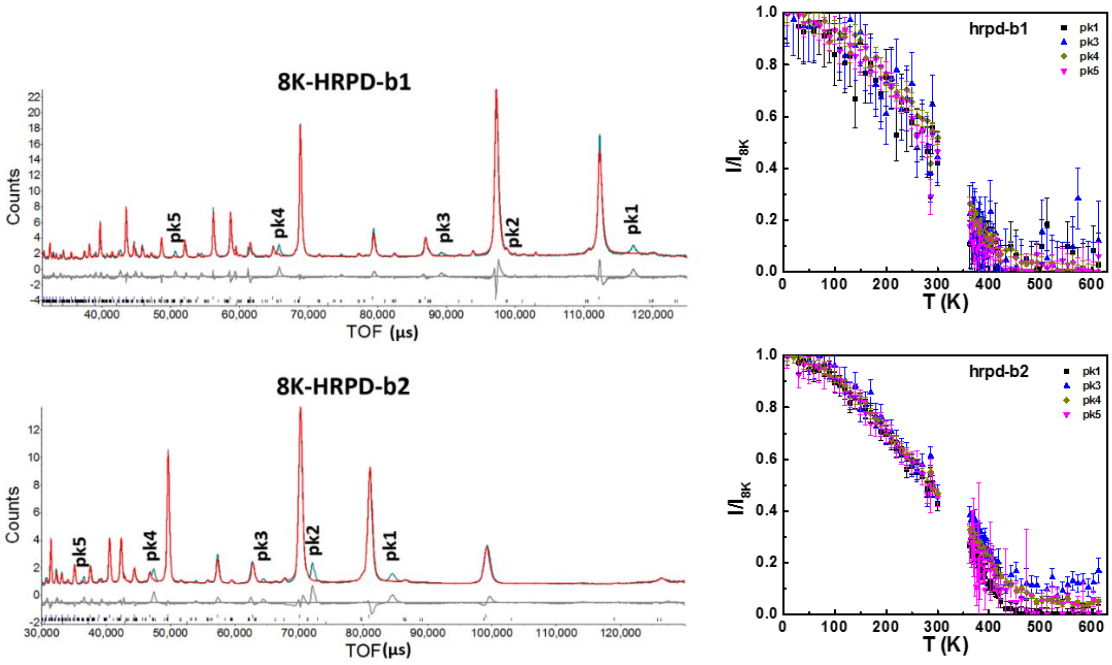

Figure 5. Neutron diffraction patterns of $SrTaO_2N$ at 8K (left, light green experiment data, red: simulated from the cubic perovskite model) and normalizes intensities of peaks marked versus temperature (right).

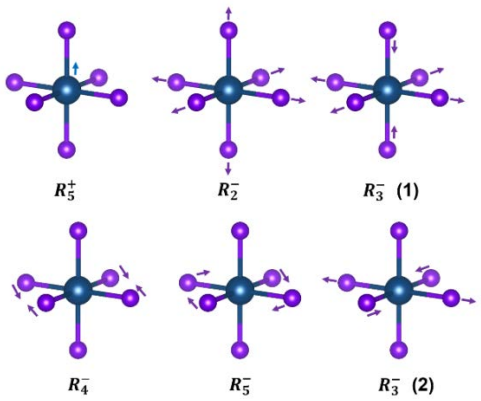

Figure 6. Illustration of the Ta-O/N octahedra displacement distortions of different **R** type IRs. For each of these, the direction of the distortion is arbitrary to the principle directions of the unit cell.

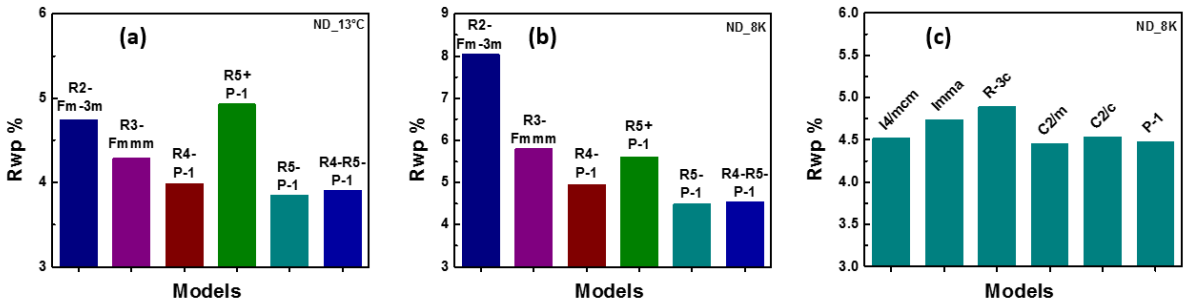

Figure 7. R_{wp} factors of the Rietveld refinements of $SrTaO_2N$ ND data using different distortion models. (a) (b) different **R** IRs with all the distortion modes refined; (c) six different structural models of $\mathbf{R}_5^-$.

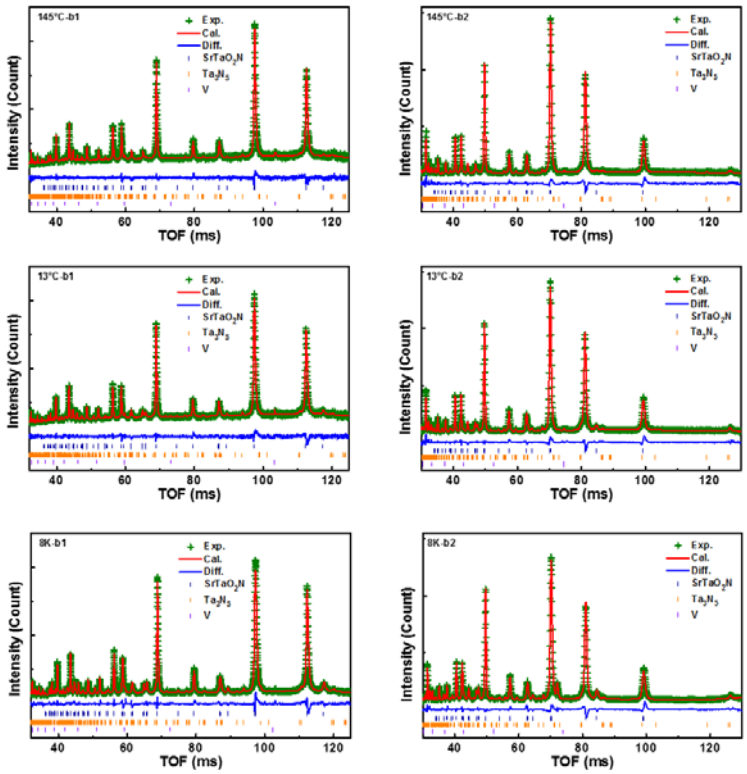

Figure 8. Refined profiles of ND data for $SrTaO_2N$ at three selected temperatures using model $\mathbf{R}_5^-$(a,0,0) *I*4/*mcm* (No 140).

The temperature dependence of the refined cell parameters of $SrTaO_2N$ is illustrated in Figure 9. As expected all the cell parameters increase with increasing temperature. The temperature dependence of the cell volume can be described by Equation 1, with the fitted parameters V_0 = 261.88(1) Å^3, C = 2.67(1) × 10^{-5} K^{-1} and θ = 275(7) K. The amplitude of Ta-O/N octahedra rotation distortion ($\mathbf{R}_5^-$ in Figure 6) is shown in Figure 9d. The distortion decreases as the temperature increases and reaches a minimum at T ~ 450 K (177 °C) showing behaviour typical of a second-order phase transition. It should be noted that the refined distortion parameter does not reach zero but ~0.1 instead, which

corresponds to ~0.03 Å in the physical space. Such a small distortion is insensitive in the refinements against the current data and can be considered negligible. Meanwhile, the cell distortion shows a similar transition accompanying with the octahedra distortion with δ decrease and showing saturation at ~ 400 K in Figure 9c. However, $\delta \neq 0$ observed after the transition temperature means that the cell distortion caused by O/N ordering remains (similar to the $BaTaO_2N$ case). As a test, we refined the ND data of $SrTaO_2N$ at 330 °C (~600 K) using $\mathbf{R}_5^-$ *I*4/*mcm* (140) and $\mathbf{\Gamma}_3^+$ *P*4/*mmm* (123) models. Both models give good fits to the experiment data with the R_{wp} factors 4.18% (overall), 3.94% (b1), 4.39% (b2) for *I*4/*mcm* model and 4.20% (overall), 3.94% (b1), 4.41% (b2) for *P*4/*mmm* model. The refined structure for both models is given as cif files in the SI. It is reasonable to conclude that around 450 K there is a structural transition from *I*4/*mcm* to *P*4/*mmm*. Additional measurements such as heat capacity are required to obtain an accurate estimate of the transition temperature.

The thermal expansion of the tetragonal cell is highly anisotropic. At all temperatures $(c_p/a_p) > 1$ as evident from Figure 9c although the individual lattice parameters expand at different rates. The final reversal is associated with the proposed *I*4/*mcm* to *P*4/*mmm* transition. Between ~ 450 and 600 K the distortion parameter $\delta = c/2 - a/\sqrt{2} = c_p - a_p$ is essentially constant. This is equivalent to the spontaneous strains described in other studies of perovskites(Tan *et al.*, 2012). Around 550 K there is a sharp increase in this and it appears that the introduction of tilting results in a greater contraction of the *a*-parameter, and the *c*-parameter is only weakly temperature dependent. The introduction of out-of-phase tilting ($Pm\bar{3}m \rightarrow I4/mcm$ transition) in perovskites such as $CaTiO_3$ (Kennedy *et al.*, 1999) and $SrZrO_3$ (Howard *et al.*, 2000) results in cell metrics $(c_p/a_p) > 1$, due to a contraction in the *ab* plane. A similar effect appears in $SrTaO_2N$ at $T < 450$ K, where the out-of-phase Ta-O/N octahedra rotation distortion caused an enhanced contraction in *ab* plane. Therefore, a strong correlation between the distortion and tetragonal cell distort (δ) was observed when the distortion is larger than 0.20, as shown in the Figure 9e.

The nature of the continuous phase transition can be established by examining the temperature dependence of the order parameter (Q), e.g., $Q = A(T_c - T)^n$ with n = ½ or ¼ for a second order or tricritical transition, respectively.(Salje, 1993) In the present case the distortion amplitude of $\mathbf{R}_5^-$ mode is a suitable order parameter. A plot of the $(\mathbf{R}_5^-)^2$ as a function of temperature is linear at high temperatures showing the transition to be second order with a transition temperature = 488(5) K. The value of $\mathbf{R}_5^-$ plateaus as T approaches 0 K due to saturation effects, and to model this, the distortion parameter (D) was fitted to expression of the type $D^2 = D_1 + D_2\theta\coth(\theta/T)$. The fit was relatively insensitive to the precise value of θ which was tried and fixed at 130 K, which is comparable to the values observed in other perovskites(Tan *et al.*, 2012). The results of this are illustrated in Figure 9d.

Table 2 Refined structure parameters of $SrTaO_2N$

T		8 K		13 °C		145 °C		330 °C	
SG		*I*4/*mcm* (140)		*I*4/*mcm* (140)		*I*4/*mcm* (140)		*P*4/*mmm* (123)	
a (Å)		5.6837(8)		5.6949(9)		5.7137(2)		4.0463(1)	
c (Å)		8.0630(12)		8.0681(14)		8.0885(10)		4.0506(4))	
V (Å^3)		260.47(11)		261.66(13)		264.06(5)		66.319(9)	
Site	Coordinate	*x* (O1/N1)	B_{eq} (Å^2)	*x* (O1/N1)	B_{eq} (Å^2)	*x* (O1/N1)	B_{eq} (Å^2)	*x* (O1/N1)	B_{eq} (Å^2)
Sr1	4b (0 ½ ¼)		0.54(3)		0.86(4)		0.95(4)	1a (0 0 0)	1.26(5)
Ta1	4c (0 0 0)		0.34(3)		0.55(4)		0.52(4)	1d (½ ½ ½)	0.73(6)
O1/N1	8h (*x*, *x*+1/2, 0)	0.7721(1)	1.27(3)	0.7666(1)	1.50(4)	0.7595(2)	1.61(4)	2e (0 ½ ½)	1.89(5)
O2	4a (0 0 ¼)		1.27(3)		1.50(4)		1.61(4)	1c (½ ½ 0)	1.89(5)

Occupancy of O1/N1 site is 0.5 O and 0.5 N. All the other sites are fully occupied.

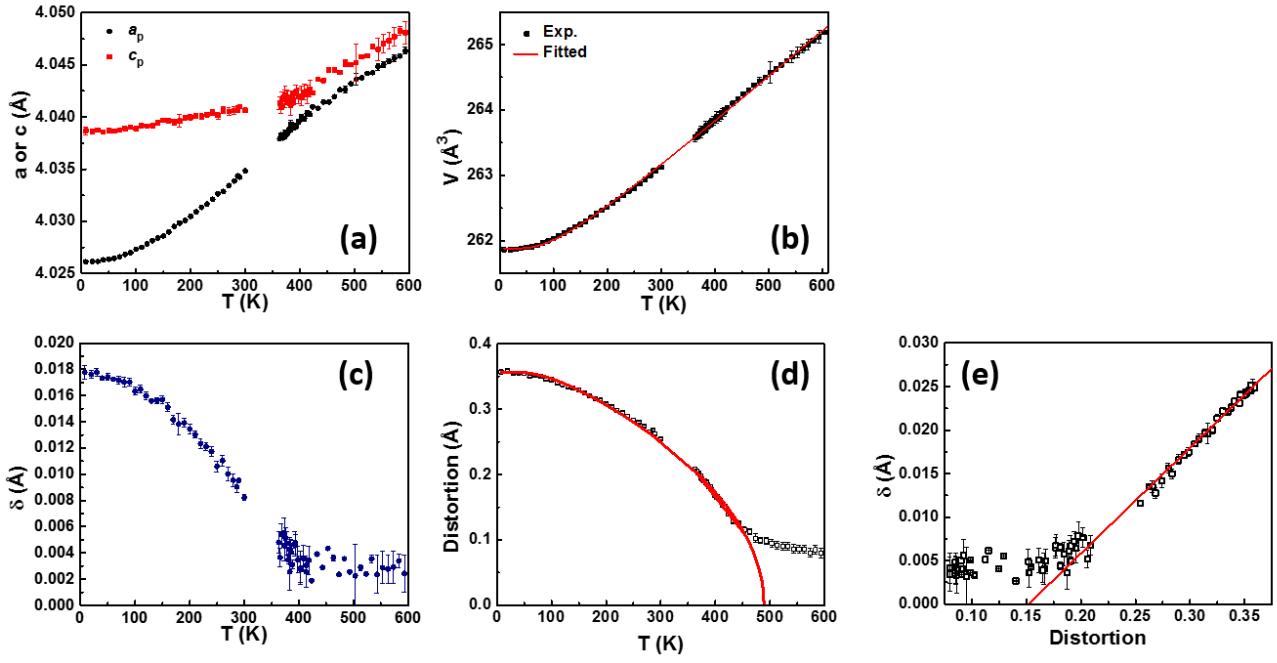

Figure 9. Temperature dependence of the appropriately scaled unit cell parameter a_p, c_p, and volume (a&b), cell distortion (c), Ta-O/N octahedra displacement distortion (d) and the correlation between distortion and cell distortion (e).

XANES of $BaTaO_2N$ and $SrTaO_2N$. XANES spectroscopy is sensitive to the local chemistry environment (valence, bond length, and coordination symmetry) of measured element. Generally, the edge energy is dominated by the valance and bond strength, whist the overall peak behaviour is dominated by the coordination symmetry. The O K-edge and N K-edge XANES TFY spectra of $BaTaO_2N$ and $SrTaO_2N$ collected at room temperature are shown in Figure 10 with the spectra normalised and smoothed. The overall O or N K-edge spectra of $SrTaO_2N$ and $BaTaO_2N$ are quite similar, which means that the coordination of O/N anion in $SrTaO_2N$ and $BaTaO_2N$ are similar. This agrees with the structure discussed above, in which 2-coordinated O or N anions sit at the corner of Ta-O/N octahedra and connect the two neighbouring octahedra. However, narrow split peaks in the range of 538 -546 eV O K-edge and 405 – 414 eV N K-edge XANES of $BaTaO_2N$ compared with that of $SrTaO_2N$ indicate that there might be subtle local structure differences between them. On the other hand, the O/N K-edge energy (compared as the energy of first peak, dash line) in $SrTaO_2N$ is ~ 0.3eV higher than that of $BaTaO_2N$. This is caused by the shorter Ta – O/N bond lengths in $SrTaO_2N$ (2.017 - 2.018 Å at RT) than those in $BaTaO_2N$ (2.055 - 2.057 Å at RT), which results in a stronger Ta – O/N bond in $SrTaO_2N$ than in $BaTaO_2N$.

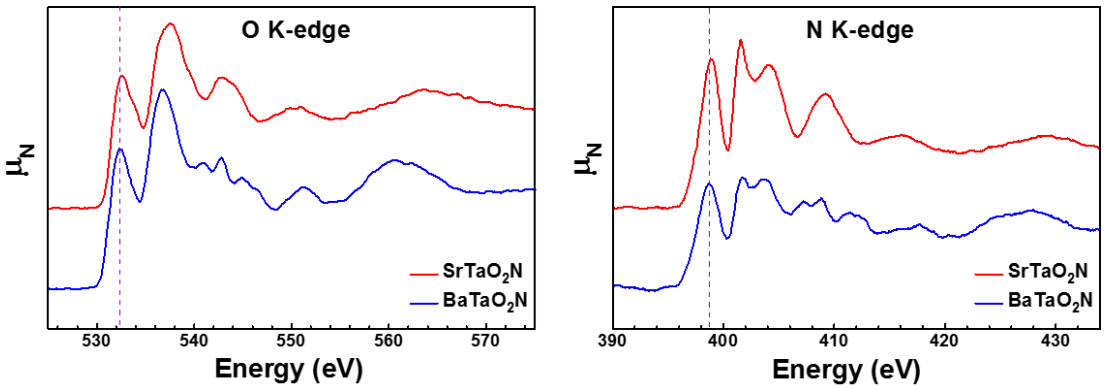

Figure 10. Normalised O/N K-edge XANES spectra of $SrTaO_2N$ and $BaTaO_2N$. The spectra were smoothed.

Optical Band gap of $BaTaO_2N$ and $SrTaO_2N$. Finally, the diffuse reflectance/absorbance spectra of $BaTaO_2N$ and $SrTaO_2N$ were also measured. For a solid material, the absorption coefficient α and the optical band gap E_g have the form(Al-Ani, 1993)

$$\alpha h\nu = C\left(h\nu - E_g\right)^n$$

where h is Planck's constant, ν is frequency of vibration, and C is a constant. The power n differs with the band gap type, e.g., n = ½ for a direct allowed band gap and n = 2 for an indirect band gap(Miller, 1995). It is not possible to determine the type of band gap from the current spectra. In Figure 11, both possibilities are plotted $(\alpha h\nu)^2 - h\nu$ and $(\alpha h\nu)^{1/2} - h\nu$ in order to derive a direct band gap E_g(d) and indirect band gap E_g(i), which are shown. For $BaTaO_2N$, the band gap is estimated to be E_g(d) = 1.78

eV and E_g(i) = 1.84 eV. The band gap of $SrTaO_2N$ is estimated to be appreciably larger E_g(d) = 1.99 eV and E_g(i) = 2.09 eV. Kim *et al.* have previously estimated the band gap of $BaTaO_2N$ and $SrTaO_2N$ to be 1.8eV and 2.1eV respectively(Kim *et al.*, 2004), which agree with our estimates of the indirect band gap. The band gap of $BaTaO_2N$ and $SrTaO_2N$ should be dominated by the orbital splitting of Ta-O/N octahedra. Since the Ta – O/N bond lengths in $SrTaO_2N$ are shorter than those in $BaTaO_2N$, $SrTaO_2N$ is expected to have a larger effective crystal field than $BaTaO_2N$ resulting in a larger orbital splitting (band gap).

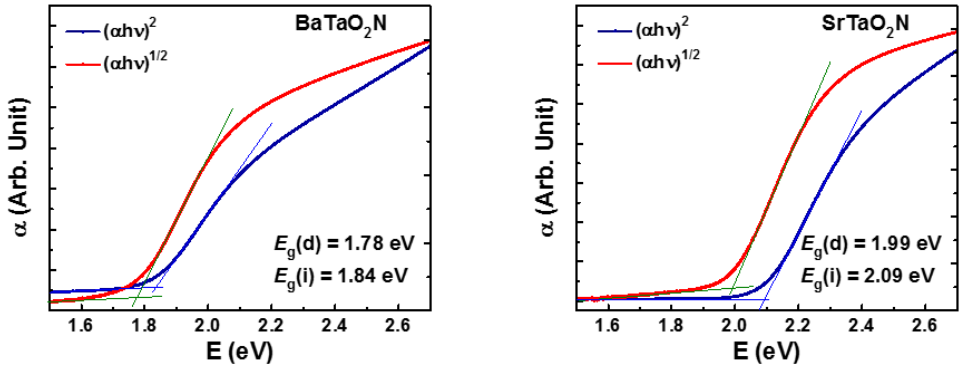

Figure 11. Absorption spectra of $BaTaO_2N$ and $SrTaO_2N$.

4. Conclusions

Polycrystalline samples of $BaTaO_2N$ and $SrTaO_2N$ were synthesized using two step high temperature solid state reaction and the structural distortions, relative to the ideal cubic perovskite structure, was analysed using high resolution neutron diffraction data. From a complete distortion analysis/refinement, different tetragonal structures were identified for $BaTaO_2N$ [*P*4/*mmm* (No 123)] and $SrTaO_2N$ [*I*4/*mcm* (No 140)] at room temperature. Ordering of the O/N anions was observed in both systems and the structural refinements show there is site occupancy preference for oxygen in the two opposite corners (along *c* axis) of the Ta-O/N octahedra than the four square corners in *ab* plane. This causes a distortion of the unit cell with the *c* axis being slightly longer than the *a* axis. In addition to this anion ordering induced distortion of the cell displacements of the anions, as a result of cooperative tilting of the Ta-O/N octahedra [$\mathbf{R}_5^-$(a,0,0) distortion mode, rotate about *c* axis], were also observed in $SrTaO_2N$. Whereas the distortion of the cell induced by anion ordering is essentially independent of temperature, the $\mathbf{R}_5^-$(a,0,0) distortion mode is temperature dependent and decreases as the temperature is increased ultimately resulting in a continuous phase transition from *I*4/*mcm* to *P*4/*mmm* around 450 K. From diffuse reflection spectra analysis, the band gap of $BaTaO_2N$ is estimated to be E_g(d) = 1.78 eV and E_g(i) = 1.84 eV. Which is somewhat smaller than in $SrTaO_2N$ E_g(d) = 1.99 eV and E_g(i) = 2.09 eV due to the longer Ta-O/N bond distances.

Acknowledgements This work was partially supported by the Australian Research Council. The measurements were conducted at the powder diffractometer and soft X-ray beamline of the Australian Synchrotron and, by a beamtime allocation from the Science and Technology Facilities Council, at the HRPD at ISIS. André Menezes would like to thank the CNPq (Process 232680/2014-0) for his postdoctoral fellowship.

References

Al-Ani, S. K. J. (1993). *Int. J. Electron.* **75**, 1153-1163.

Attfield, J. P. (2013). *Crystal Growth & Design* **13**, 4623-4629.

Campbell, B. J., Stokes, H. T., Tanner, D. E. & Hatch, D. M. (2006). *J. Appl. Crystallogr.* **39**, 607-614.

Clark, L., Oro-Sole, J., Knight, K. S., Fuertes, A. & Attfield, J. P. (2013). *Chem. Mater.* **25**, 5004-5011.

Clarke, S. J., Hardstone, K. A., Michie, C. W. & Rosseinsky, M. J. (2002). *Chem. Mater.* **14**, 2664-2669.

Coelho, A. A., Evans, J. S. O., Evans, I. R., Kern, A. & Parsons, S. (2011). *Powder Diffr.* **26**, S22-S25.

Evans, J. S. O. (2010). *Extending the reach of powder diffraction modelling by user defined macros*, edited by P. Scardi & R. E. Dinnebier, pp. 1-9.

Fang, C. M., de Wijs, G. A., Orhan, E., de With, G., de Groot, R. A., Hintzen, H. T. & Marchand, R. (2003). *J. Phys. Chem. Solids* **64**, 281-286.

Günther, E., Hagenmayer, R. & Jansen, M. (2000). *Z. Anorg. Allg. Chem.* **626**, 1519-1525.

Higashi, M., Abe, R., Teramura, K., Takata, T., Ohtani, B. & Domen, K. (2008). *Chem. Phys. Lett.* **452**, 120-123.

Higashi, M., Domen, K. & Abe, R. (2013). *J. Am. Chem. Soc.* **135**, 10238-10241.

Higashi, M., Yamanaka, Y., Tomita, O. & Abe, R. (2015). *Apl Materials* **3**,

Hinuma, Y., Moriwake, H., Zhang, Y.-R., Motohashi, T., Kikkawa, S. & Tanaka, I. (2012). *Chem. Mater.* **24**, 4343-4349.

Howard, C. J., Knight, K. S., Kennedy, B. J. & Kisi, E. H. (2000). *J. Phys.: Condens. Matter* **12**, L677.

Kennedy, B. J., Howard, C. J. & Chakoumakos, B. C. (1999). *J. Phys.: Condens. Matter* **11**, 1479.

Kerman, S., Campbell, B. J., Satyavarapu, K. K., Stokes, H. T., Perselli, F. & Evans, J. S. O. (2012). *Acta Crystallogr. A* **68**, 222-234.

Kim, Y.-I., Woodward, P. M., Baba-Kishi, K. Z. & Tai, C. W. (2004). *Chem. Mater.* **16**, 1267-1276.

Lewis, J. W., Payne, J. L., Evans, I. R., Stokes, H. T., Campbell, B. J. & Evans, J. S. O. (2016). *J. Am. Chem. Soc.* **138**, 8031-8042.

Masubuchi, Y. (2013). *J. Ceram. Soc. Jpn.* **121**, 142-149.

Miller, A. (1995). *Handbook of optics, volume i: Fundamentals , techniques , and design*, edited by M. Bass, E. W. V. Stryland, D. R. Williams & W. L. Wolfe, pp. 9.1-9.33. New York: McGRAW-HILL , INC .

Oehler, F. & Ebbinghaus, S. G. (2016). *Solid State Sci.* **54**, 43-48.

Page, K., Stoltzfus, M. W., Kim, Y.-I., Proffen, T., Woodward, P. M., Cheetham, A. K. & Seshadri, R. (2007). *Chem. Mater.* **19**, 4037-4042.

Pors, F., Marchand, R., Laurent, Y., Bacher, P. & Roult, G. (1988). *Mater. Res. Bull.* **23**, 1447-1450.

Ravel, B., Kim, Y. I., Woodward, P. M. & Fang, C. M. (2006). *Phys. Rev. B* **73**, 184121.

Salje, E. K. H. (1993). *Phase transitions in ferroelastic and co-elastic crystals*. Cambridge: Cambridge University Press.

Sun, S.-K., Zhang, Y.-R., Masubuchi, Y., Motohashi, T. & Kikkawa, S. (2014). *J. Am. Ceram. Soc.* **97**, 1023-1027.

Talanov, M. V., Shirokov, V. B. & Talanov, V. M. (2016). *Acta Crystallogr. A* **72**, 222-235.

Tan, T.-Y., Kennedy, B. J., Zhou, Q., Ling, C. D., Miiller, W., Howard, C. J., Carpenter, M. A. & Knight, K. S. (2012). *Phys. Rev. B* **85**, 104107.

Ueda, K., Minegishi, T., Clune, J., Nakabayashi, M., Hisatomi, T., Nishiyama, H., Katayama, M., Shibata, N., Kubota, J., Yamada, T. & Domen, K. (2015). *J. Am. Chem. Soc.* **137**, 2227-2230.

Wolff, H. & Dronskowski, R. (2008). *J. Comput. Chem.* **29**, 2260-2267.

Yang, M. H., Oro-Sole, J., Rodgers, J. A., Jorge, A. B., Fuertes, A. & Attfield, J. P. (2011). *Nature Chemistry* **3**, 47-52.

Zhang, Y.-R., Motohashi, T., Masubuchi, Y. & Kikkawa, S. (2011). *J. Ceram. Soc. Jpn.* **119**, 581-586.

Supporting information

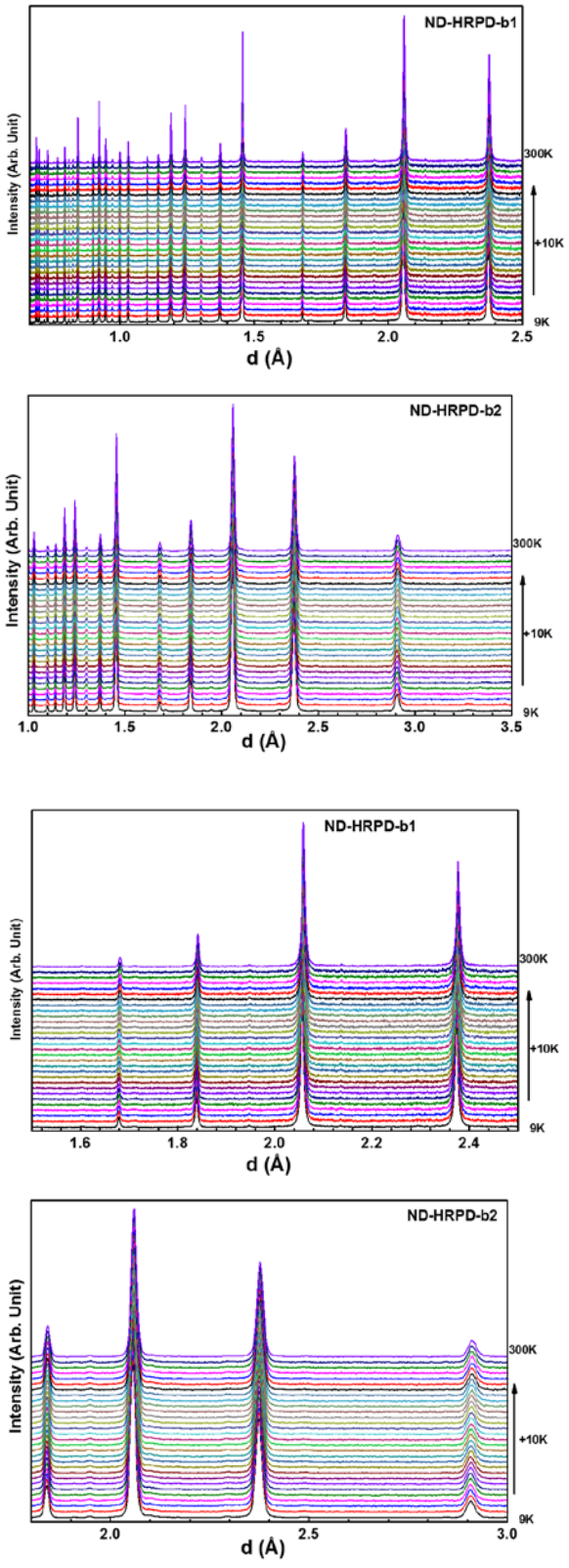

Figure S1 Variable temperature neutron diffraction patterns of $BaTaO_2N$.

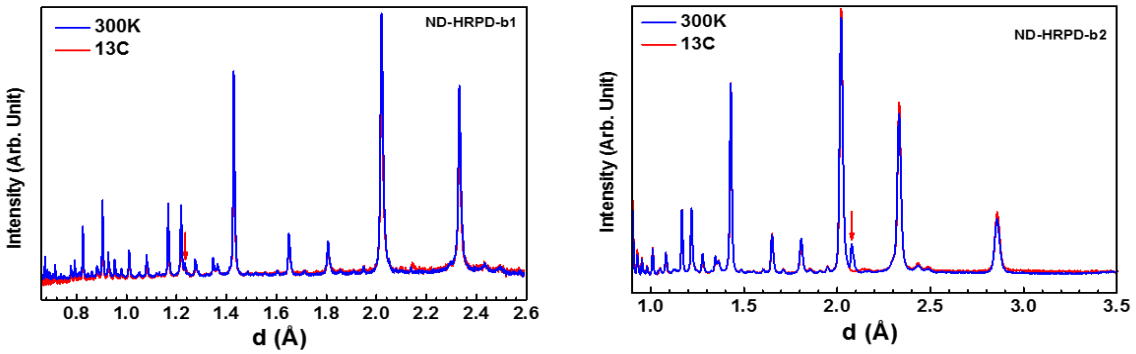

Figure S2 Neutron diffraction patterns of $SrTaO_2N$ at 300 K and 13 °C.

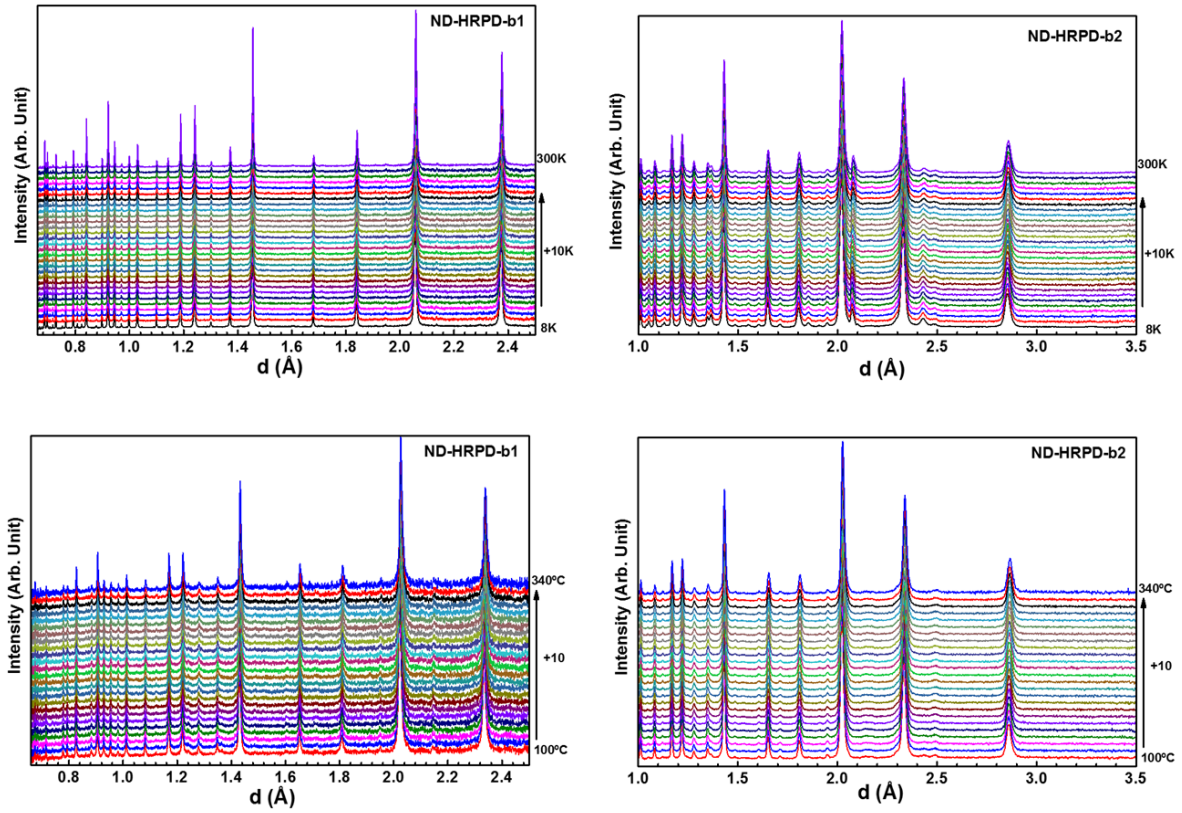

Figure S3 Variable temperature neutron diffraction patterns of $SrTaO_2N$.